

Characterization of wax as a potential diffraction intensity standard for macromolecular crystallography beamlines

J. Brandao-Neto,^{a*} S. P. Thompson,^a A. R. Lennie,^b F. F. Ferreira^c and C. C. Tang^a

^aDiamond Light Source, Harwell Science and Innovation Campus, Didcot, Oxfordshire, UK, ^bSTFC Daresbury Laboratory, Warrington WA4 4AD, UK, and ^cLaboratório Nacional de Luz Síncrotron, CP 6192, CEP 13083-970, Campinas, Brazil. E-mail: jose.brandao-neto@diamond.ac.uk

A number of commercially available waxes in the form of thin disc samples have been investigated as possible diffraction intensity standards for macromolecular crystallography synchrotron beamlines. Synchrotron X-ray powder diffraction measurements show that beeswax offers the best performance of these waxes owing to its polycrystallinity. Crystallographic lattice parameters and diffraction intensities were examined between 281 and 309 K, and show stable and predictable thermal behaviour. Using an X-ray beam of known incident flux at $\lambda = 1 \text{ \AA}$, the diffraction power of two strong Bragg reflections for beeswax were quantified as a function of sample thickness and normalized to 10^{10} photons s^{-1} . To demonstrate its feasibility as a diffraction intensity standard, test measurements were then performed on a new third-generation macromolecular crystallography synchrotron beamline.

Keywords: beeswax; macromolecular crystallography; MX intensity standard; synchrotron powder diffraction.

1. Introduction

1.1. Macromolecular crystallography diffraction standards

There are in the region of 100 macromolecular crystallography (MX) beamlines either operational or being commissioned at synchrotron radiation sources worldwide (Djinović Carugo *et al.*, 2005). Intended to address high-profile scientific challenges, these powerful instruments are designed to solve large complex protein structures. Such instruments require good quality standard calibration materials in order to allow the recording of accurate scientific data. Although standard specimens are available for calibrating instruments in almost every field, and reference samples for X-ray powder diffraction are produced specifically for calibration of beam quality (wavelength/energy and intensity) and instrumental accuracy (angular position), there are currently no widely accepted standards available for calibration of MX instruments.

Hen egg-white lysozyme is widely used as a macromolecular crystal analogue when commissioning instruments (Kitago *et al.*, 2005; Jakoncic *et al.*, 2006; Ravelli *et al.*, 2007; Shimizu *et al.*, 2007). It crystallizes readily, even in the presence of cryoprotectant, and its size and morphology can be controlled (Forsythe *et al.*, 1999); growth times for lysozyme crystals are typically three to four days (Chayen, 1998). Although stabilization by cross-linking can increase resilience (Mueller-Dieckmann *et al.*, 2005), lysozyme crystals are still susceptible

to radiation damage (Shimizu *et al.*, 2007). Furthermore, after cross-linking, lysozyme scattering characteristics can be somewhat variable (Lusty, 1999; Mueller-Dieckmann *et al.*, 2005). Commercial stabilized lysozyme crystals (*e.g.* Molecular Dimensions Ltd) may offer a reasonable starting point for assessing a given MX experiment, but are not ideal as quantitative diffraction intensity standards for assessing beamline parameters. Insulin (Dix *et al.*, 2006), trypsin and thaumatin (Yang *et al.*, 2003) and elastase (*e.g.* Xenocs Application Note, DMC-061207) have also been used as diffraction standards in MX experiments. However, the processed diffraction signal from such crystals often contains artefacts owing to the combined effects of the source, beamline, sample, goniometer, detector and analysis software (Arndt & Wonnacott, 1977; Walker & Stuart, 1983; Bourenkov & Popov, 2006).

As each of these materials has difficulties associated with availability, preparation, stability, durability and repeatability, we consider that there is a clear need in MX for a stable, robust, high-quality and easily reproducible standard intensity calibration material.

1.2. Requirements of an MX reference standard

MX samples are typically protein assemblies and are polymeric crystals with densities of $\sim 1.2 \text{ g cm}^{-3}$, unit-cell dimensions which vary from tens to hundreds of angstroms (Ladd & Palmer, 2003) and have an amorphous content that varies

between 10% and 90%. These crystals typically comprise 50:50 H₂O:C ratios, which for 1 Å radiation gives an X-ray linear absorption length close to 5 mm. Any standard for testing MX instrumental performance should ideally be based on a material with similar physical properties.

When only relative changes in electron density maps are being measured, the use of single crystals such as lysozyme is understandable. However, in experiments where performance of the source, optics and detector are important factors, such crystals are not ideal for calibration since their morphology cannot be chosen *a priori*. Anisotropic crystals can result in unwanted features in recorded X-ray data, such as uncontrolled modulations in diffraction patterns, which are difficult to model (Walker & Stuart, 1983).

By contrast, calibrated reference materials for diffraction, such as silicon (SRM 640c, NIST) and LaB₆ (SRM 660a), are specifically produced for determining precise powder line position and shape (Cline *et al.*, 2000). These are accepted as 'gold' standards for the calibration of wavelength, 2θ zero-point offset and instrumental resolution of powder diffraction beamlines at synchrotron radiation facilities. While such standards are important for quantitative assessments of data quality from a given experimental arrangement (Wong-Ng & Hubbard, 1987), they are not good analogues for MX crystals in terms of scattering power. In addition, loose powders are unsuitable for intensity standards because diffracted strength is dependent on the packing density of the material. Other intensity standards such as sintered alumina (SRM 1976) and the intensity set CeO₂, Cr₂O₃, TiO₂ and ZnO (SRM 674b) are not easily manipulated for transmission characterization measurements. Such standards do not provide the means for simulating MX signal-to-noise ratios, exposure times and recorded intensities.

1.3. Waxes as candidate reference materials

The waxy material silver behenate [CH₃(CH₂)₂₀COOAg] is widely used as a small-angle X-ray scattering standard (Suortti *et al.*, 1985; Huang *et al.*, 1993) owing to low-angle 00*l* peaks arising from large *d*-spacings (e.g. *d*₀₀₁ = 58.38 Å). Unfortunately, the small crystallite size (~900 Å) results in significant line broadening, making it unsuitable as a standard for higher angle measurements. While beeswax has, for example, previously been used in MX to determine X-ray beam centres during image-plate data processing (e.g. *MOSFLM*; Leslie, 1992), waxes also have potential as polycrystalline MX analogues since many of their physical properties are similar to MX samples. Despite a long cell parameter in only one direction (~150 Å), the density of wax (<1 g cm⁻³) is close to typical MX crystals owing to close packing in the other directions (~10 Å). For the X-ray exposure times commonly required for MX crystals (e.g. 0.5–20 s in third-generation synchrotrons; 1–20 min in rotating anodes), background levels and peak heights for waxes also appear comparable with those from MX crystals. Moreover, in contrast to MX crystal morphology, wax samples can be moulded easily to a known shape or size, allowing comparison of data from equivalent

samples collected on different instruments. These properties make the use of wax as a potential MX intensity standard worthy of further investigation.

In this paper we describe the method of sample production and the synchrotron radiation X-ray work needed to identify a wax with properties best suited for a potential MX diffraction intensity standard. Although waxes may be derived from many sources (animal, vegetable, mineral, petroleum and synthetic), the object of this paper is not to conduct a comprehensive survey of the properties and suitability of all possible waxes but to propose a candidate that has consistency in its manufactured quality, ease of supply and diffraction quality. We address the characterization of polycrystalline phases in terms of crystallinity, powder quality, thermal stability and X-ray attenuation.

2. Experimental procedure

Synchrotron X-ray measurements were performed in four stages using different beamlines for specific tasks:

(i) The crystallinity and particle distribution of each wax was screened using station 9.5HPT (SRS, Daresbury Laboratory, UK; Lennie *et al.*, 2007) to identify which of the waxes studied represented the most suitable candidate and determine its thermal behaviour over a range of temperatures typical of ambient conditions in synchrotron radiation experimental hutches. Station 9.5HPT receives X-rays from a 5 T superconducting wiggler inside the 2 GeV electron storage ring, with monochromatic X-rays obtained using a Laue focusing Si(111) crystal located 30 m from the source. Diffraction patterns are recorded with a mar345 image plate ~343 mm behind the sample position, with the actual sample-to-plate distance calibrated using the diffraction pattern of SRM 640c Si powder and *Fit2d* software (Hammersley *et al.*, 1996; Hammersley, 1997). The absorption edge of an indium foil ($\lambda = 0.44397$ Å) placed close to the monochromator was used to calibrate the energy of the focused X-ray beam (60 μm × 60 μm).

(ii) The diffraction strengths (intensities) of the strong Bragg peaks of the candidate wax identified from stage (i) above, along with its attenuation characteristics, were then measured using beamline D10B-XPD at the LNLS (Brazil). This is a scanning geometry powder diffraction beamline with a double-bounce Si(111) monochromator (Ferreira *et al.*, 2006) located on a 1.67 T bending-magnet beamline in the 1.37 GeV synchrotron ring. D10B-XPD was selected for this stage since the incident flux at the sample position has been accurately quantified *via* calibrated diode detector (Ferreira *et al.*, 2006). The wavelength of the incident beam (1 mm × 2 mm) was tuned to 1.0 Å and calibrated ($\lambda = 0.9997 \pm 0.0004$ Å) using diffraction data from Si SRM 640c powder.

(iii) The long-term storage stability of the selected sample and its survival in a high-intensity X-ray beam was tested using the I11 powder diffraction beamline (Tang *et al.*, 2007; Thompson *et al.*, 2009) at the 3 GeV Diamond synchrotron. Sourced by a 90-pole in-vacuum undulator, I11 receives high photon rate [e.g. $5.7 \times 10^{13} \text{ s}^{-1}$ (0.1% bandpass)⁻¹ (250 mA)⁻¹

at 10 keV] monochromatic X-rays (5–30 keV) within a sample area of $\sim 1 \text{ mm} \times 4 \text{ mm}$. Diffraction data are collected *via* five multi-analyzer crystal stages, equipped with Si 111 analyzer crystals. Measurements using this beamline were made approximately one year after the D10B-XPD beam time. In the interim, the samples were stored at room temperature (296 K) in plastic containers.

(iv) Finally, to demonstrate the potential of the candidate wax as an MX diffraction intensity standard, test measurements were made on MX beamline I04 at Diamond, also sourced by an in-vacuum undulator. Kirkpatrick–Baez focusing mirrors deliver a low-bandpass high-brightness X-ray beam to the sample position (Sorensen *et al.*, 2006). Diffraction patterns were recorded in rotation camera geometry (Arndt & Wonnacott, 1977) using an ADSC Q315r CCD area detector 500 mm behind the sample position and a calibrated wavelength of $\lambda = 0.970 \text{ \AA}$.

2.1. Sample preparation

For this study, four easily obtainable commercial waxes were investigated: beeswax (Hampton Research HR4-312), nonadecane (Aldrich N28906, 99%), dotriacontane (Aldrich D223107, 97%) and *n*-docosane (Aldrich 134457, 99%). Moulding into small sample discs, placed perpendicular to the X-ray beam, allowed all measurements to be made in transmission. This provides a short distance for the beam to traverse, minimizing absorption effects, while allowing the whole beam to impinge on the sample, improving data collection times and statistics.

Stainless steel discs were used as both moulds and support for the waxes. The discs were $0.50 \pm 0.05 \text{ mm}$ thick and had a $10.0 \pm 0.1 \text{ mm}$ diameter bore machined at the centre. These were laid on a flat metal tray held at 340 K, while the waxes were melted at the same temperature and poured into the disc holes until the liquid was level with the disc rim. Both were then allowed to cool to room temperature. Fig. 1 shows two of the prepared samples. This method produces samples with variable thicknesses ($t = 0.4\text{--}1.1 \text{ mm}$), suitable for the synchrotron radiation powder diffraction measurements.

The preparation method was later improved to produce samples of any desired thickness between 500 and 1000 μm with high precision. Melted raw material was poured into a $10 \text{ mm} \times 10 \text{ mm} \times 25 \text{ mm}$ ($\pm 0.1 \text{ mm}$ in each direction) aluminium mould. When released, the resulting wax block was cut using a microtome blade (RMC MT990) and the thickness of the resulting disc checked using high-precision digital callipers. Measured thicknesses were found to be accurate to within $\pm 3 \mu\text{m}$.

3. Results

3.1. Crystallographic suitability and thermal stability (SRS station 9.5HPT)

A diffraction intensity standard should possess randomly orientated submicrometre crystallites of good crystallinity. Samples of the four selected waxes were therefore screened



Figure 1
Examples of the prepared wax samples (diameter = 10 mm, thickness $\simeq 0.4\text{--}1.1 \text{ mm}$) inside stainless steel discs.

for this on station 9.5HPT. Fig. 2 shows diffraction patterns for each wax. In terms of good crystallinity and absence of texture, *i.e.* uniform powder rings, it is clear that the candidate most suited for further investigation is beeswax (Fig. 2*d*). Six thin beeswax specimens were then prepared from the same starting material and further diffraction data obtained from two of these for crystallographic characterization.

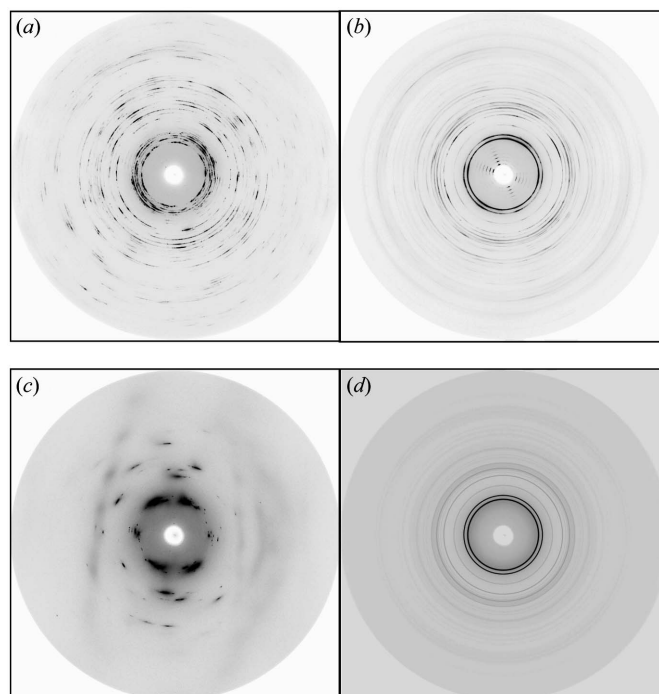


Figure 2
Diffraction patterns of the wax samples measured on station 9.5HPT at $\lambda = 0.44397 \text{ \AA}$: (a) *n*-docosane, (b) dotriacontane, (c) nonadecane and (d) beeswax. Only the beeswax sample produces uniform powder rings characteristic of a good polycrystalline material.

Table 1

Refined lattice parameters of beeswax and average crystallite size (σ).

Beeswax	a (Å)	b (Å)	σ (nm)
Specimen #01	7.4516 (7)	4.9705 (5)	72 (2)
Specimen #02	7.4525 (7)	4.9715 (5)	72 (2)

Powder profiles of intensity versus 2θ for beeswax were produced by integrating around the Debye–Scherrer rings in the two-dimensional images using *Fit2d*. Cell parameters were obtained by Le Bail profile refinement (Le Bail, 1992) using *TOPAS (General Profile and Structure Analysis Software for Powder Diffraction Data, DIFFAC-plus, version 3.0, Bruker)*.

Previously, Basson & Reynhardt (1988) found that commercial beeswax gave a powder diffraction pattern identical to Fischer–Tropsch medium wax, which crystallizes in orthorhombic form. We therefore obtained good refinements in space group $Pca2_1$ (No. 29) using the fundamental instrumental parameters approach (Cheary & Coelho, 1992) where beam size and source–sample–detector distances are used to deconvolute peak shapes to extract average crystallite size. Fig. 3 shows the refinement, with $R_{wp} = 5.56\%$, for one diffraction profile. Obtained lattice parameters and crystallite sizes for the two specimens are summarized in Table 1. Within refinement errors, the unit-cell dimensions and particle sizes are in close agreement. Owing to the long unit cell edge of the c -axis (~ 132 Å), the strong low-order ($00l$) peaks were not detectable using the 9.5HPT beamline configuration and the c -parameter was not included in the refinement. The relative strength of the two dominant 110 and 200 peaks should be noted, as these are used later in the calibration of diffracted intensity.

Basson & Reynhardt (1988) also observed steep changes in the unit cell of beeswax between 80 and 320 K. Since a wax standard could be used at different maintained temperatures (e.g. SPring-8: 301 K; Diamond: 296 K), its thermal depen-

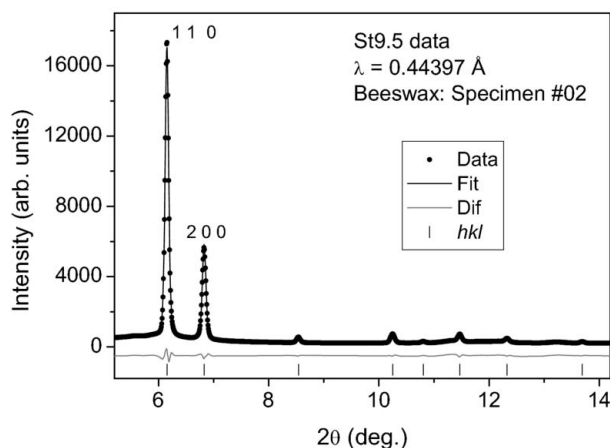


Figure 3

Integrated diffraction profile of a beeswax sample (specimen #02) measured at room temperature (294 K) using station 9.5HPT. The Le Bail refinement (solid line) shows the fit to data (points) using an orthorhombic unit cell. The strong 110 and 200 peaks used to characterize the diffraction strength of beeswax are labelled.

ency must be characterized. The variation in lattice parameters between $T = 281$ and 303 K was measured by diffraction for specimen #01 using an Oxford 700 series cryostream to control sample temperature (Fig. 4a). Although significant shifts are observed, the changes within this range are predictably described by a linear function. More importantly, the variations in the diffracted signals for the 110 and 200 reflections are small [Fig. 4(b) for peak maxima and Fig. 4(c) for integrated intensities], the largest and smallest spreads being in the 200 peak intensity ($\leq 4.5\%$) and 110 integrated intensity ($\leq 2\%$).

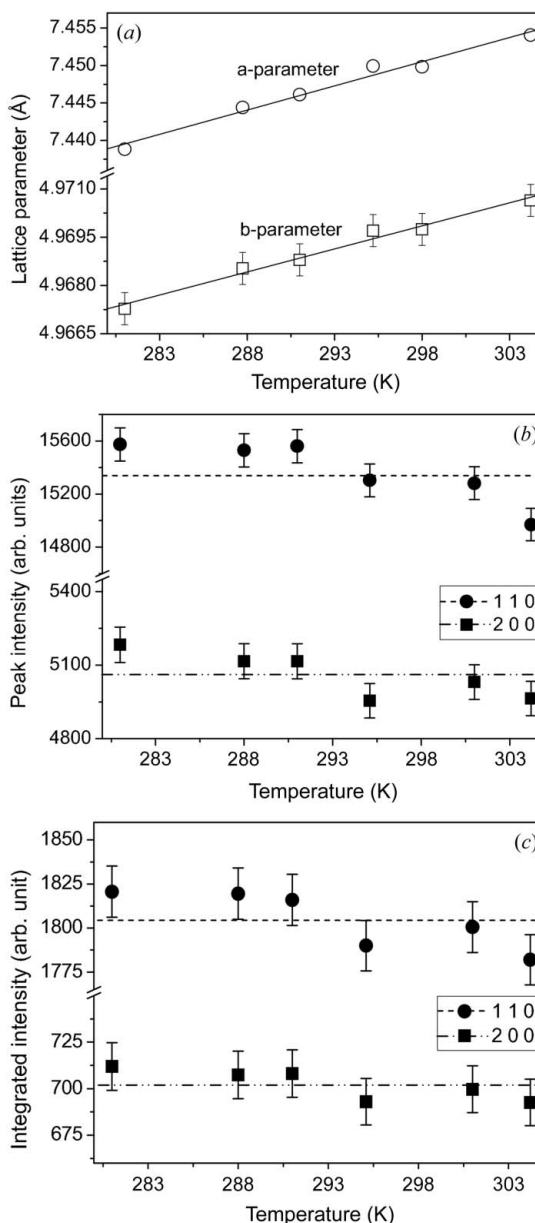


Figure 4

(a) Refined lattice parameters as a function of temperature for beeswax (station 9.5HPT data). The straight lines are linear fits to the data sets and the error bars for the a parameter are smaller than the plotted point. (b) Peak intensity as a function of temperature for the 110 and 200 reference reflections. (c) Integrated intensity as a function of temperature. Dashed lines show the averaged values.

3.2. Diffraction intensity and attenuation characteristics (LNLS D10B-XPD)

For this stage, the instrument was set up in low-resolution mode with a set of slits 91 cm from the sample position and 0.6 mm (vertical) by 30 mm (horizontal) collimation slits in front of a Cyberstar X1000 (Oxford Danfysik) detector. With appropriate shaping time and gain the efficiency of the detector is expected to be >95% at 12.4 keV, with a good linear response up to 3×10^5 counts s^{-1} . In order to normalize or calibrate measured intensities from the wax specimens, it was crucial to first know the photon flux of the incident X-ray beam as a function of energy. This is shown in Fig. 5, measured some months earlier using a calibrated photodiode (Ferreira *et al.*, 2006). However, the figure also shows a value of 5.6×10^9 photons s^{-1} (100 mA) $^{-1}$ for the flux measured, using the same diode, at the start of our experiment for the tuned wavelength (~ 12.4 keV in the figure) and is consistent with adjacent points on the curve. Since the measurement relies on the calibration procedure and corrections for absorption and efficiency, which are the main sources of uncertainty, the derived flux is expected to have an error of up to 5%.

3.2.1. Attenuation characteristics. Several thicker beeswax samples (~ 10 mm diameter \times 3 mm thick) were made for determining the X-ray attenuation. With a measured density of $\rho = 0.93$ (1) $g\ cm^{-3}$, an absorption coefficient $\mu = 1.09$ (1) cm^{-1} (half thickness, $t_{1/2} \simeq 7.6$ mm) was obtained at the tuned wavelength. Sample thicknesses (Table 2) were calculated from X-ray transmission using $I = I_0 \exp(-\mu t)$ and also measured using precision callipers; both show good agreement.

3.2.2. Diffraction intensity. Since the incident beam photon flux is known, the diffraction strength of the wax specimens can be measured. The 110 and 200 peaks were measured by step scanning 2θ at $0.005^\circ\ s^{-1}$ with the synchrotron beam current recorded at the start and end of each scan. Since the flux at 100 mA of electron beam current is known, all data can be normalized to that current or flux. However, measurements

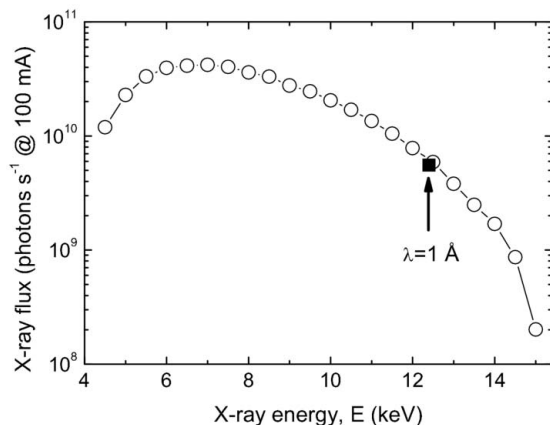


Figure 5 Previously measured photon flux, as a function of X-ray energy, for D10B-XPD per 100 mA storage ring current. The filled square arrowed at $E = 12.4$ keV ($\lambda = 1$ Å) is the flux measured at the start of the D10B-XPD beam time.

Table 2

Calculated and measured thicknesses (t) of beeswax specimens.

$$\mu = 1.09$$
 (1) cm^{-1} , $\rho = 0.93$ (1) $g\ cm^{-3}$.

Beeswax specimen	t (caliper) (mm)	t (X-ray) (mm)
#01	1.10 (1)	1.11 (1)
#02	0.89 (1)	0.899 (9)
#03	0.91 (1)	0.936 (9)
#04	1.04 (1)	1.04 (1)
#05	0.58 (1)	0.599 (7)
#06	†	0.425 (5)

† Direct measurement was not made since the sample is thinner than the holding disc.

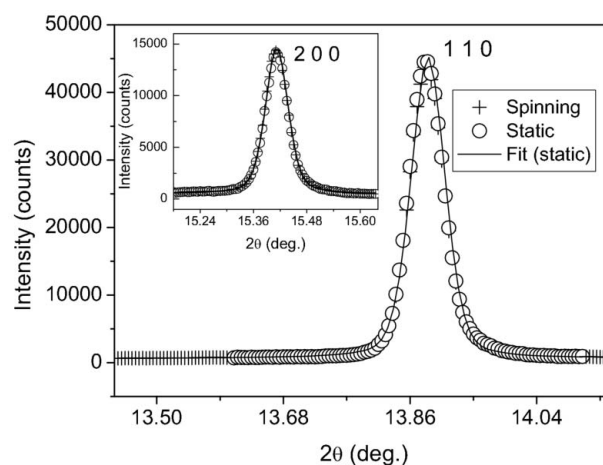


Figure 6

The 110 (main plot) and 200 (inset) reflections scaled to 10^{10} photons s^{-1} measured from beeswax specimen #01. These peaks measured for spinning and non-spinning (static) specimen on D10B-XPD are presented together for comparison purposes. The data were fitted with a pseudo-Voigt function (solid lines).

at other synchrotrons can also be compared if our data are scaled to the flux of 10^{10} photons s^{-1} provided by the bandpass of the monochromator, $\Delta\lambda/\lambda \simeq 2 \times 10^{-4}$, which is typical for most MX beamlines. Therefore, the 110 and 200 profiles normalized to the decade power are shown in Fig. 6 for specimen #01 [$t = 1.10$ (2) mm]. In powder work it is usual to improve particle averaging by spinning or rotating samples in the beam and Fig. 6 also contrasts peak profiles obtained from static and spinning samples. The absence of any discernible difference confirms the good polycrystalline nature of beeswax. As peak strength also depends on sample thickness, the reflections were measured for all specimens and their intensities scaled accordingly to establish the thickness dependency. The diffraction strength can be represented by either peak (per 2θ step) or integrated intensity as shown in Fig. 7. Here, the background for each peak profile has been subtracted for the integration analysis and, with known detector aperture and distance from the sample (angle of detection, $\delta = 1.196^\circ$), the results have been normalized to unit angle. This is necessary to allow comparison with area detectors, where near-full Debye–Scherrer rings are recorded and peaks integrated by $\sim 360^\circ$ to give two-dimensional patterns. As Fig. 7 shows, with the small spread of specimen thicknesses

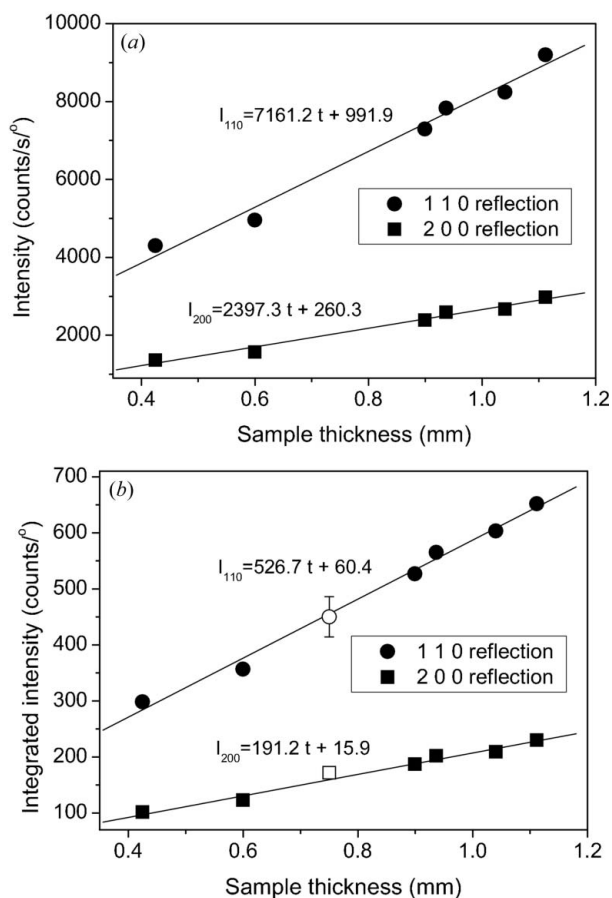


Figure 7 Diffraction strength of 110 (filled circles) and 200 (filled squares) reflections measured on D10B-XPD powder beamline as a function of specimen thickness: (a) peak intensity and (b) integrated intensity. I04 MX data corrected to account for differences in beamline and instrumental details (§3.4) are also plotted as an open circle (110) and open square (200) in (b). All data have been scaled to 10^{10} photons s^{-1} and the angle (per degree) of detection. Note that for the D10B-XPD and I04 (200) data the error bars are smaller than the plotted points.

and with $t_{1/2} \gg t$, intensity and thickness exhibit a linear relationship for each peak.

3.3. Durability and radiation hardness (Diamond I11)

To test both the beeswax stability when exposed to a high-intensity beam and its stability in long-term storage, 43 consecutive diffraction scans of specimen #02 were made over a 13 h period using 12 keV X-rays. Fig. 8 shows the 110 and 200 peak intensities as a function of time; neither peak shows any degradation with time. The statistical spread in intensity for each peak is consistent with counting statistics. In addition, a and b lattice parameters were refined for the first and last data set and are shown in the top left and right of the figure, respectively. Again, no appreciable difference is observed and leads us to conclude that beeswax does not suffer when exposed to high-intensity beams. Furthermore, comparing the I11 diffraction patterns with the earlier 9.5HPT data showed no indication of the sample having aged between experiments.

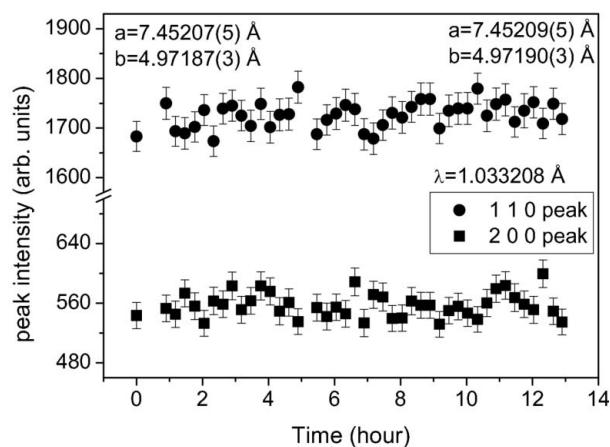


Figure 8 Stability of the 110 and 200 peak intensities when exposed to a high-intensity X-ray beam on I11 at Diamond. Each point represents a single scan. Missing points at ~ 0.5 and ~ 5.25 are due to storage ring refill.

3.4. MX test measurements (Diamond I04)

From the results thus far, beeswax samples between $t = 0.4$ and $t = 1.1$ mm thick should be suitable for use as a diffraction intensity standard on a typical MX beamline. Although it is not usually straightforward to compare directly data from two instruments with different detection systems, source characteristics and experimental arrangements, it is necessary to demonstrate the equivalence between the measurements reported here for the D10B-XPD powder beamline and those obtainable from a typical MX beamline.

A diffraction pattern was collected from a new specimen, with $t = 0.750 \pm 0.003$ mm, using a $0.2 \text{ mm} \times 0.2 \text{ mm}$ beam and 1 s exposure. At the start of the measurement an incident flux of 5×10^{11} photons s^{-1} (with $\sim 5\%$ error) at the sample was recorded using a calibrated photodiode and for the purpose of comparison and diffraction data from a $100 \mu\text{m}$ -wide pixel strip in the vertical scattering plane were extracted.

To compare like with like we have to consider the differences between the I04 and D10B-XPD measurements and then apply any necessary corrections in order to scale the results accordingly. Since a detailed rigorous analysis of the beam characteristics and scattering geometries of the two beamlines would be beyond the scope of this paper, we employ the following semi-qualitative approach to correct and normalize the data from the two instruments.

First, the extracted I04 intensities expressed in analogue-to-digital conversion units (ADU) need to be converted to photon counts. Assuming 100% scintillation efficiency for the CCD detector, the front-end gain is 8.5 electrons per 12.4 keV X-ray photon, with a conversion gain of 3.36 electrons per ADU. Hence, the strength of the peaks can be converted into intensity counts since a single X-ray photon generates 2.5 analogue–digital units. Second, the difference in acceptance angle (δ) in the vertical scattering plane and the amount of powder ring collected for both beamlines must be accounted for, *i.e.* the diffracted intensity normalized per degree of the acceptance angle in the horizontal plane (χ). The incident

Table 3
Correction factors (CF) for normalization of the integrated intensities.

	D10B-XPD	I04	CF
Transmission factor and detector efficiency, τ	100%	79%	1.27
Vertical acceptance angle (δ)	0.038°	0.011°	3.43
Combined correction factor, $CF_C = 4.36$			
110 peak ($2\theta = 13.488^\circ$)			
Horizontal acceptance angle (χ)	1	0.0478°	20.93
Peak width (β)	0.0572°	0.0441°	1.30
Peak/background (η)	87.2	50.0	1.74
Combined correction factor, $CF_{110} = 47.34$			
200 peak ($2\theta = 14.980^\circ$)			
Horizontal acceptance angle (χ)	1°	0.0428°	23.35
Peak width (β)	0.060°	0.047°	1.28
Peak/background (η)	39.4	21.48	1.83
Combined correction factor, $CF_{200} = 54.70$			

Table 4
Combined correction factors and I04 integrated intensities.

	1 1 0	2 0 0
Combined correction factor, $CF_C CF_{hkl}$	206.42	238.47
Integrated intensity, I_{OBS} ($^\circ \text{ s}^{-1}$)	109	36
Corrected integrated intensity, I_{COR} ($^\circ \text{ s}^{-1}$)	22500	8585
I_{COR} normalized to 10^{10} photon s^{-1}	450	172

X-ray beams used for the measurements also have different divergences as observed in their peak widths (β), which must be corrected for. The contrast between peak and background for the D10B-XPD scanning mode using collimation slits should be better than the I04 CCD pixel measurements without detector collimation. Therefore the difference in peak/background ratios (η) must be taken into account. Finally, I04 has a longer air path than D10B-XRD and the different transmission effect needs to be considered. This can be combined with the differences in the detector efficiency into a single parameter (τ).

In this way, the observed intensities, I_{OBS} , measured on I04 can be corrected using $I_{COR} = (CF_C CF_{hkl}) I_{OBS}$, where $CF_C = \tau\delta$ and $CF_{hkl} = \chi\beta\eta$, with δ , χ , β , η and τ expressed as ratios of the D10B-XPD to I04 parameters (see Table 3). The correction was only applied to the integrated intensity for each peak (Table 4) as this is a more reliable quantity. After flux normalization (to 10^{10} photon s^{-1}), including the corrected values, Fig. 7(b) shows the corrected I04 MX values to be in good agreement with the D10B-XPD powder data. The individual error bar plotted for the normalized intensity is about 8% owing to contributions from the measured flux ($\sim 5\%$) and the associated uncertainties in the corrected datum ($\sim 3\%$).

4. Discussion

Any standard material must meet certain basic criteria. It needs to be straightforward to work with in terms of handling or preparation; robust both in terms of its ability to cope with the conditions of use (e.g. exposure to X-rays, temperature

stability) and its resistance to long-term ageing. It must also be fit for purpose, which in the current context means it needs to possess good polycrystalline characteristics and well characterized diffraction strength. From the samples studied, commercial beeswax appears to exhibit better polycrystalline properties than the synthetic waxes examined, *i.e.* the random distribution of small submicrometre crystallites yields strong uniform powder rings. In this respect beeswax is a good candidate for an MX intensity reference. Beeswax also meets the ease of handling and preparation criteria and we have described a routine method for the manufacture of suitable samples that does not require specialist equipment or conditions. Furthermore, we have shown that the beeswax samples used in this study do not degrade either from natural ageing or from exposure to the high-intensity X-ray beams typical of third-generation sources. We have characterized the thermal dependency of beeswax as a function of the 281 to 304 K temperature range typical of synchrotron facilities, showing that the lattice parameters on the a - b plane exhibit a predictable linear behaviour within this range, while the two strongest 110 and 200 peak intensities remain largely unaffected.

We have characterized the diffraction and attenuation properties of beeswax samples with thicknesses, t , between 0.4 and 1.1 mm using powder diffraction and normalized to the incident flux of the $\lambda = 0.9907 \text{ \AA}$ X-ray beam for a given electron beam current. The absorption coefficient [$\mu = 1.09 (1) \text{ cm}^{-1}$] and half thickness ($t_{1/2} \simeq 7.6 \text{ mm}$) were obtained and, for samples where $t \ll t_{1/2}$, the integrated and peak intensity (normalized to 10^{10} photons s^{-1}) as a function of thickness is shown to give a linear variation.

Once differences in beamline geometry, detector and source characteristics are accounted for, we have demonstrated the parity between the diffraction strength as measured using powder and MX methods. The sample preparation method, intensity benchmarking and other measurements (sample thickness and attenuation coefficient) clearly indicate the suitability of beeswax for use as an intensity reference for the calibration and testing of MX beamlines.

We have not investigated the possibility that beeswax obtained from a different source might exhibit different characteristics to the ones we report. However, we do not believe this to be a significant consideration. Beeswax is classified generally into European and Oriental types, reflecting the evolutionary divergence of bee species in the Late Miocene period. Kameda (2005), for example, found that Japanese beeswax in its as-secreted state contains a mixture of orthorhombic and triclinic (or monoclinic) structures. However, beeswax destined for commercial use undergoes purification by recrystallization. Here, melting the natural product in hot water, filtering to remove insoluble materials, followed by controlled cooling and subsequent recrystallization, results in the orthorhombic structures commonly reported by other researchers. Beeswax is composed of long-chain carbon components, including alkanes with 21 to 33 C atoms, acids with 22 to 30 C atoms and esters with 40 to 52 C atoms. European and Oriental beeswax differ in their sapo-

nification values, which is essentially a measure of the average carbon chain length and is lower for European beeswax. Differences in chain length should, however, affect only those properties directly related to the *c*-axis lattice parameter. Since we have deliberately characterized only those lattice parameters from the *a*-*b* plane and scattering intensity originating from this plane, such differences are unlikely to impact on the results presented here.

We would like to acknowledge Laboratório Nacional de Luz Síncrotron (LNLS) for the provision of beam time (6451/07) and technical staff for their kind assistance during our experiment. We thank the Directors of the SRS, Daresbury Laboratory, for allocation of beam time (49156) for this study. Our thanks go to Dr Ralf Flaig and Dr Dave Waterman for their assistance in our experiment on beamline I04 at Diamond, and to Dr Alice Douangamath for early tests on alkane samples and sample holders.

References

- Arndt, U. W. & Wonnacott, A. J. (1977). *The Rotation Method in Crystallography*. Amsterdam: North Holland.
- Basson, I. & Reynhardt, E. C. (1988). *J. Phys. D*, **21**, 1421–1428.
- Bourenkov, G. P. & Popov, A. N. (2006). *Acta Cryst.* **D62**, 58–64.
- Chayen, N. E. (1998). *Acta Cryst.* **D54**, 8–15.
- Cheary, R. W. & Coelho, A. (1992). *J. Appl. Cryst.* **25**, 109–121.
- Cline, J. P., Deslattes, R. D., Staudenmann, J.-L., Kessler, E. G., Hudson, L. T., Henins, A. & Cheary, R. W. (2000). NIST Certificate, *SRM 640c Line Position and Line Profile Standard for Powder Diffraction*. National Institute of Standards and Technology, Gaithersburg, MD 20899, USA.
- Dix, I., Rühl, S., Fink, L. & Sheldrick, G. M. (2006). *Acta Cryst.* **A62**, s21.
- Djinović Carugo, K., Helliwell, J. R., Stuhmann, H. & Weiss, M. S. (2005). *J. Synchrotron Rad.* **12**, 410–419.
- Ferreira, F. F., Granado, E., Carvalho Jr, W., Kycia, S. W., Bruno, D. & Droppa Jr, R. (2006). *J. Synchrotron Rad.* **13**, 46–53.
- Forsythe, E. L., Nadarajah, A. & Pusey, M. L. (1999). *Acta Cryst.* **D55**, 1005–1011.
- Hammersley, A. P. (1997). *FIT2D: An Introduction and Overview*, Technical Report ESRF97HA02T. European Synchrotron Radiation Facility, Grenoble, France.
- Hammersley, A. P., Svensson, S. O., Hanfland, M., Fitch, A. N. & Hausermann, D. (1996). *High Press. Res.* **14**, 235–248.
- Huang, T. C., Toraya, H., Blanton, T. N. & Wu, Y. (1993). *J. Appl. Cryst.* **26**, 180–184.
- Jakoncic, J., Di Michiel, M., Zhong, Z., Honkimaki, V., Jouanneau, Y. & Stojanoff, V. (2006). *J. Appl. Cryst.* **39**, 831–841.
- Kameda, T. (2005). *J. Phys. D*, **38**, 4313–4320.
- Kitago, Y., Watanabe, N. & Tanaka, I. (2005). *Acta Cryst.* **D61**, 1013–1021.
- Ladd, M. & Palmer, R. (2003). *Structure Determination by X-ray Crystallography*, 4th ed., p. 678. New York: Kluwer Academic/Plenum Publishers.
- Le Bail, A. (1992). *Accuracy in Powder Diffraction II*, NIST Special Publication No. 846, edited by E. Prince and J. K. Stalick, p. 213. Gaithersburg: US Department of Commerce.
- Lennie, A. R., Laundy, D., Roberts, M. A. & Bushnell-Wye, G. (2007). *J. Synchrotron Rad.* **14**, 433–438.
- Leslie, A. G. W. (1992). *Jnt CCP4/ESF-EACMB Newsl. Protein Crystallogr.* **26**.
- Lusty, C. J. (1999). *J. Appl. Cryst.* **32**, 106–112.
- Mueller-Dieckmann, C., Panjikar, S., Tucker, P. A. & Weiss, M. S. (2005). *Acta Cryst.* **D61**, 1263–1272.
- Ravelli, R. B. G., Haselmann-Weiss, U., McGeehan, J. E., McCarthy, A. A., Marquez, J. A., Antony, C., Frangakis, A. S. & Stranzl, G. (2007). *J. Synchrotron Rad.* **14**, 128–132.
- Shimizu, N., Hirata, K., Hasegawa, K., Ueno, G. & Yamamoto, M. (2007). *J. Synchrotron Rad.* **14**, 4–10.
- Sorensen, T. L.-M., McAuley, K. E., Flaig, R. & Duke, E. M. H. (2006). *Trends Biotechnol.* **24**, 500–508.
- Suortti, P., Hastings, J. B. & Cox, D. E. (1985). *Acta Cryst.* **A41**, 413–416.
- Tang, C. C., Thompson, S. P., Hill, T. P., Wilkin, G. R. & Wagner, U. H. (2007). *Z. Kristallogr. Suppl.* **26**, 153–158.
- Thompson, S. P., Parker, J. E., Potter, J., Hill, T. P., Birt, A., Cobb, T. M., Yuan, F. & Tang, C. C. (2009). *Rev. Sci. Instrum.* **80**, 075107.
- Walker, N. & Stuart, D. (1983). *Acta Cryst.* **A39**, 158–166.
- Wong-Ng, W. & Hubbard, C. R. (1987). *Powder Diffr.* **2**, 242–248.
- Yang, C., Pflugrath, J. W., Courville, D. A., Stence, C. N. & Ferrara, J. D. (2003). *Acta Cryst.* **D59**, 1943–1957.